Electrochimica Acta 427 (2022) 140870

Contents lists available at ScienceDirect

Electrochimica Acta

journal homepage: www.journals.elsevier.com/electrochimica-acta

Ultrathin ion-selective membranes for trace detection of lead, copper and silver ions

Kequan Xu [1], Yujie Liu [1], Gaston A. Crespo, Maria Cuartero [*]

Department of Chemistry, School of Engineering Science in Chemistry, Biotechnology and Health, KTH Royal Institute of Technology. Teknikringen 30, Stockholm SE-100 44, Sweden

ARTICLE INFO

Keywords:
Ultrathin ion-selective membrane
Voltammetric ion-selective electrode
Trace metals
Charge transfer
Water samples

ABSTRACT

Voltammetric ion-selective electrodes (ISEs) based on poly(3-octylthiophene) (POT) in connection with ultrathin membranes formulated with different selective receptors (i.e., ionophores) are proposed for detection of lead, copper and silver ions (Pb^{2+}, Cu^{2+} and Ag^{+}). The working mechanism of the POT-membrane electrode is based on interconnected charge transfer processes on both sides of the membrane, with the overall process depending on the electron transfer in the POT lattice ultimately linked to the ion transfer at the membrane–sample interface. This latter is demonstrated to be controlled by (i) the membrane composition and (ii) the accumulation/stripping electrochemical protocol, allowing the detection of traces of Ag^{+}, Pb^{2+} and Cu^{2+}. In the case of the Pb^{2+}-selective electrode, the voltammogram displays several peaks that are hypothesized to correspond to different ion–ionophore stoichiometries. Following the signal related to the principal stoichiometry (1:1), a Pb^{2+} concentration as low as 0.1 nM is measurable. In contrast, the Cu^{2+}- and Ag^{+}-selective electrodes show only one peak for the corresponding ion analyte, which can be also detected at nanomolar concentrations. The results obtained with the three electrodes support their further usage for multi-ion detection in water samples through either a multi-ionophore-based electrode or multiple-electrode device. In any case, the membrane composition, in terms of the ionophore/exchanger molar ratio, is key to achieving a successful analytical application. Upcoming efforts may be directed at the replacement of traditional trace metal ion detection with the hanging mercury drop electrode to develop a more sustainable electrochemical approach without diminishing the analytical performance.

1. Introduction

Heavy metals are traditionally defined as naturally occurring elements that have a high atomic weight and a density at least five times greater than that of water [1]. They can be found in the environment at different levels and in certain manufactured products, pharmaceuticals and food, among others [2]. Some heavy metals (e.g., copper, iron and zinc) are indeed micronutrients, needed by organisms in varying but small quantities to orchestrate a range of physiological functions, while others (such as mercury) have been identified as very toxic or tracers of human-generated pollution (e.g., silver, lead and arsenic) [3]. There may be a fine line between a given heavy metal being safe or dangerous, and thus, permissible levels have been established for their ionic forms when dissolved in water, which is the main mean by which they reach living organisms (including human beings) [4]. As a first measure, to prevent exposure of human beings to heavy metal ions and avoid any adverse effects such ions may have on aquatic systems, it is advisable to accurately control the concentrations in environmental waters. It is also useful to test for heavy metals in other samples, including food and beverages, pharmaceuticals, biological fluids and tissues.

Among the analytical techniques available for the detection of heavy metals, electrochemistry has gained importance in the past decade because the different redox activity of these ions permits their simultaneous detection in a single scan round. In addition, electrochemical sensors have many favorable characteristics, including their suitability for miniaturization and automation, ease of use, cost effectiveness and high compatibility with on-site measurements [3]. The combination of mercury electrodes with anodic stripping voltammetry detection seems to yield particularly good analytical performance. The hanging mercury drop electrode (HMDE) is commercially available for the simultaneous

* Corresponding author.
E-mail address: mariacb@kth.se (M. Cuartero).
[1] These authors contributed equally to this work.

https://doi.org/10.1016/j.electacta.2022.140870
Received 14 March 2022; Received in revised form 31 May 2022; Accepted 16 July 2022
Available online 17 July 2022

detection of several heavy metals (Zn^{2+}, Cd^{2+}, Pb^{2+} and Cu^{2+}) at the nanomolar level with excellent accuracy and reproducibility. The first submersible probe for *in situ* usage in freshwater and seawater was reported in 1990, and was based on a sessile mercury drop electrode together with a mercury film electrode for the detection of Zn^{2+}, Cd^{2+}, Pb^{2+} and Cu^{2+} [5]. The most advanced version of such a device (the so-called Voltammetric *in-situ* profiler, VIP, from Idronaut) [6] comprises an on-chip microelectrode array with interconnected iridium micro-discs modified with electrochemically coated Hg microlayers and can detect Zn^{2+}, Cd^{2+}, Pb^{2+} and Cu^{2+} at ppt levels, as well as Fe^{2+} and Mn^{2+} at ppb levels.

Despite the excellent performance of mercury-based electrodes for trace metal analysis, there are some important drawbacks to their use, including the high toxicity of mercury, together with their inability to detect silver, mercury and gold ions —because their signals overlap with the oxidation of the mercury electrode— as well as other metal ions that are not able to form stable amalgams with mercury (e.g., Ni^{2+}, Co^{2+} and Cr^{4+}) [7,8]. These limitations have encouraged the development of other types of electrodes. Many efforts have been dedicated to the search for new electrode materials, highlighting the utilization of noble metals (e.g., platinum and silver), bismuth and antimony [9,10]. Unfortunately, the use of the HMDE is still the recommended analytical technique in reference laboratory analysis [11], which reflects the difficulty of identifying new electrode types that can match its performance for heavy metal detection. Most such electrodes fail in the detection of Zn^{2+} and/or Cu^{2+}. Noble metals have a limited cathodic potential window because of H_2 formation at low potentials, which hinders the determination of Zn^{2+}, while bismuth and antimony usually present narrow anodic windows limited by the oxidation of the metal film *per se*, which prevents the detection of Cu^{2+}. Peak distortions, in the form of shoulders, double peaks and/or overlapping, are very common and affect the detection of Pb^{2+} in particular. This behavior has been attributed to the formation of intermetallic compounds (e.g., Pb-Cu [12,13] and Cu-Hg [14]). In addition, electrodes tend to display linear ranges of responses at the micromolar level [8,13,15–17], and their fabrication and maintenance processes are usually too complicated for many labs and end users.

All-solid-state ion-selective electrodes (ISEs) based on ultra-thin membranes have been developed in recent years for use in the detection of various ions during a voltammetric scan, without the ions needing to display redox activity [18]. The electrode is tailored with a solid contact material —specifically, poly(3-octylthiophene), or POT— whose oxidation state is gradually changed upon application of a linear sweep potential, i.e., POT^0 is converted to POT^+. The generated charge (POT^+) provokes a redistribution of the ions already present in the membrane, resulting in the expulsion of cations to the solution. The process consists of a series of interconnected charge transfer events, including electron transfer in the POT lattice and ion transfer at the membrane–sample interface. The ion transfer can be tuned to be selective for one or more cations, given the simultaneous incorporation of up to three selective receptors (ionophores) in the membrane [18,19]. Despite the evident potential of this analytical approach to multi-ion detection, its application to heavy metal analysis has not yet been demonstrated, to the best of our knowledge. Another interesting feature of the concept described above relies on the compatibility with an accumulation/stripping methodology, which makes it possible to obtain limits of detection in the nanomolar range [20,21]. At such low concentrations, the ion analyte dynamically accumulates in the membrane, depending on its diffusion from the bulk sample solution. The accumulation involves a concentration profile at the membrane–sample interface that favors ion accumulation in the membrane with increasing time, rotation and ion concentration in the solution, until the exchange capacity of the membrane is fully utilized. At the optimized accumulation conditions, the voltammetric peak was found to increase with the ion analyte concentration in the sample at (sub)nanomolar levels [20,21].

Inspired by these results, we investigated the analytical performance of voltammetric ISEs based on ultra-thin membranes configured to be selective for Pb^{2+}, Cu^{2+} or Ag^+. This is, to the best of our knowledge, the first time that a set of heavy metals has been determined with such a technology. The three cations were selected to demonstrate that the proposed electrodes have the potential for challenging detections, such as that of Ag^+, Pb^{2+} and Cu^{2+}, as justified above. We studied the individual response of each electrode with the accumulation/stripping electrochemical method using different membrane compositions to potentiate the response down to the nanomolar level. In addition, we (semi-empirically) examined the possibility of using the electrodes herein developed as part of an all-in-one sensor whose membrane contains the three ionophores for Pb^{2+}, Cu^{2+} and Ag^+ or as part of a multiple-electrode device.

2. Experimental

2.1. Reagents, instrumentation and electrodes

Aqueous solutions were prepared in ultrapure water (18.2 MΩ, Milli-Q purification system). All the containers used in this study were treated with 10% HNO_3 overnight before and after each experiment and then washed with an ample amount of water. Even with such a cleaning process, sometimes it was difficult to remove all traces of lead, which was found to slightly influence our experiments, especially concerning the voltammograms in a pure background solution. Lead nitrate ($Pb(NO_3)_2$), copper nitrate ($Cu(NO_3)_2$), silver nitrate ($AgNO_3$), 3-octylthiophene (OT, 97%), sodium nitrate ($NaNO_3$), high-molecular-weight poly (vinyl chloride) (PVC), bis(2-ethylhexyl)sebacate or dioctyl sebacate (DOS), sodium tetrakis[3,5-bis(trifluoromethyl)phenyl]borate (Na^+TFPB^-), lead ionophore IV (PbIP), copper ionophore I (CuIP), silver ionophore IV (AgIP), acetonitrile (ACN) and tetrahydrofuran (>99.9%, THF) were purchased from Sigma-Aldrich.

Glassy carbon GC-electrode tips (Model 6.1204.300) with an electrode diameter of 3.00 ± 0.05 mm were sourced from Metrohm. Stripping voltammograms were recorded with a PGSTAT128N (Metrohm Autolab B.V., Utrecht, The Netherlands) controlled by Nova 2.0 software (supplied by Autolab). A double junction Ag/AgCl/3 M KCl/1 M LiOAc reference electrode (Model 6.0726.100, Metrohm, Switzerland) and a platinum electrode (Model 6.0331.010, Metrohm, Switzerland) were used in a three-electrode cell as reference and counter electrodes, respectively. The applied potential in all experiments described herein is referred to as the Ag/AgCl reference electrode. A rotating disk electrode (Model EDI 101, LANGE, Switzerland) was used to spin coat the membrane on the electrode at 1500 rpm and for the electrochemical measurements in the accumulation/stripping protocol. All the experiments were obtained in triplicate (three similar electrodes) to confirm the validity of the results. However, no further calculations were conducted to evaluate the reproducibility, since this was not necessary for the fundamental studies presented in this paper.

The electrodes were prepared as described elsewhere, by electrodeposition of a film of POT (0.1 M OT solution in 0.1 M $LiClO_4$ and ACN background, two cyclic voltammetry scans, 0–1.5 V, 100 mV s^{-1}, and then discharging at 0 V for 120 s) into the GC electrode tip, and later modification with the thin film of the membrane (by depositing 25 µL of a diluted THF-based cocktail while rotating the electrode at 1500 rpm) [20]. Diluted THF-based cocktails were obtained by mixing 50 µL of a parent membrane cocktail with 150 µL of THF. **Table 1** summarizes the compositions of the parent membranes, expressed in terms of the amount of each compound (i.e., PVC as the polymer, DOS as the plasticizer, NaTFPB as the cation-exchanger and either PbIP, CuIP or AgIP as the ionophore) dissolved in 1 mL of THF. The electrodes were not further conditioned, but immediately used after preparation.

For the potentiometric measurements with a traditional lead-selective electrode, this was prepared by modifying a GC electrode tip with carbon nanotubes as the ion-to-electron transducer

Table 1
Compositions of the parent (undiluted) membrane cocktails. PbIP, CuIP and AgIP refer to lead, copper and silver ionophores, respectively. The amounts are expressed in mg.

Membrane	PVC	DOS	NaTFPB	PbIP	CuIP	AgIP	IP/NaTFPB molar ratio
MI	30	60	3.44	4.00	–	–	40:40
MII	30	60	1.72	8.00	–	–	80:20
MIII	30	60	0.86	8.00	–	–	80:10
MIV	30	60	3.44	–	2.10	–	40:40
MV	30	60	1.72	–	4.20	–	80:20
MVI	30	60	3.54	–	–	6.38	80:40
MVII	30	60	1.74	–	–	6.26	80:20

(octadodecylammonium-based nanotubes synthesized as reported elsewhere [22], drop casting of 1 mg mL^{-1} in THF, 10 µL x 10 times, waiting until THF evaporation before each deposition), and then, with the lead-selective membrane on top (50 µL x 5 times, waiting until THF evaporation before each deposition of a membrane cocktail containing approximately 33 mg of PVC, 66 mg of DOS, 1.4 mg of PbIP and 0.6 mg of NaTFPB in 1 mL of THF [23]). The electrode was conditioned in 1 mM $Pb(NO_3)_2$ overnight and then in 1 nM $Pb(NO_3)_2$ solution for two days before usage [23].

3. Results and discussion

The concept of multi-ion transfer is illustrated in Fig. 1**a** for three cations (A^+, B^+ and C^+). The membrane in the electrode is composed of three ionophores, and hence, it is a kind of "all-in-one sensor," responsive to several cations. Since each cation presents a different binding constant with a corresponding ionophore, different energies are required to generate different cation transfers. Hence, the voltammogram displays three separate peaks, appearing in the order of increasing ion-ionophore binding strength (Fig. 1**b**) [18]. The global mechanism for generating cation stripping from the membrane is based on the application of a linear sweep potential, wherein the basal state of POT^0 is oxidized to POT^+, which is stabilized with the $TFPB^-$ present in the membrane (from the cation exchanger Na^+TFPB^-), with the concomitant expulsion of cations across the membrane driven by electroneutrality maintenance. If an accumulation step is incorporated before the stripping, the total amount of Na^+ initially present in the membrane is partially or totally replaced by those cations from the solution for which the membrane is selective. As the cation concentration is increased in the solution, the replacement degree increases, and its diffusion from the solution to the membrane is promoted until the total exchanged is reached at a certain concentration. From that point, the regime for the response mechanism of the system changes from diffusion-control to thin-layer behavior, i.e., no mass transport limitation in the solution. Accordingly, the stripping peak is found to initially

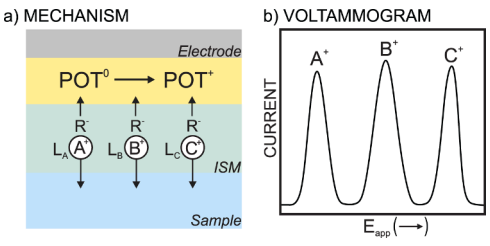

Fig. 1. (a) Illustration of the working mechanism of electrodes composed of the POT-membrane tandem. L_A, L_B and L_C represent three different ionophores that are selective for A^+, B^+ and C^+ cations, respectively. R^- represents the anionic lipophilic part of the cation exchanger in the membrane. **(b)** Example of a voltammogram observed for three different ion transfers assisted by three different ionophores simultaneously incorporated into the membrane (corresponding to Fig. 1**a**).

increase and then shift with increasing concentration in the sample solution [24].

Of note is that, in principle, the accumulation step will only work in conditions where the ion analyte is at very low concentration in the sample solution, so that the conditions for ion diffusion in the solution phase can be tuned to control in turn an increasing accumulation in the membrane at a convenient applied potential with increasing concentration in the solution. Such accumulation potential is also essential to ensure the recovery of the initial state of the electrode: at 0 V any oxidized POT^+ returns to POT and the membrane is expected to be as originally prepared.

3.1. Response of the lead-selective electrode prepared with membranes containing different ionophore/exchanger ratios

Fig. 2 presents the stripping voltammograms for membranes containing PbIP/NaTFPB in molar ratios of 40:40 (MI), 80:20 (MII) and 80:10 (MIII) at increasing Pb^{2+} concentrations (from 0.05 to 500 nM) in a 10 mM $NaNO_3$ background solution. The 40:40 ratio was selected for the first round of experiments because this is the composition traditionally used in the corresponding potentiometric ISEs (i.e., 2:2 ionophore:NaTFPB molar ratio) [23]. The other two membrane compositions were subsequently tested to evaluate the effect of decreasing the NaTFPB content on the electrode voltammetric response. To visualize any effect related to the decrease of the NaTFPB amount with respect to the ionophore (i.e., a decrease in the exchange capacity of the membrane), the content of the latter was doubled in the two membranes. Note that the conditions for the accumulation/stripping protocol were fixed as described in the literature [21]; for the accumulation step, $E_{app} = 0$ V for t = 720 s at a rotation speed of 2500 rpm; for the stripping step, a linear sweep potential from 0 to 1.2 V at a scan rate of 100 mV s^{-1}.

Fig. 2**a** shows the results for the 40:40 PbIP/NaTFPB membrane (MI). As observed in the voltammogram for the background solution ($NaNO_3$), there is one peak at 407 mV *(Peak 1)* assigned to the Na^+ transfer at the membrane–sample interface, as there is no other cation in the solution. The peak current of such a peak was found to gradually decrease with the first addition of Pb^{2+} in the sample solution, until it disappeared at a concentration of 7 nM Pb^{2+}. The peak position was rather well maintained in the range of 407–419 mV. Another peak appeared at 751 mV *(Peak 2)*, when the Pb^{2+} concentration was increased to 0.07 nM in the solution. This peak continued to increase until a concentration of 10 nM Pb^{2+} was reached in the solution (Fig. 2**b**), while the peak potential gradually shifted to less positive values (from 751 to 664 mV). This shift suggests that the Pb^{2+} transfer from the membrane to the solution becomes more energetically favorable with increasing Pb^{2+} concentration in the membrane. Nevertheless, a further increase (up to 500 nM) resulted in a gradual decrease in the peak current, until a shoulder in the baseline was reached, with the peak potential remaining almost constant (658–649 mV). In a first attempt, this peak is evidently ascribed to the presence of Pb^{2+} in the sample solution, and it is surely related to a transfer assisted by the ionophore. Otherwise, for a non-assisted transfer, the peak would have appeared at a potential slightly lower than that for the Na^+ peak, as expected for double-charged cations [25]. Another Pb^{2+} peak *(Peak 3)* started to emerge at 940 mV from the 0.3 nM Pb^{2+} concentration, whose current gradually increased with the Pb^{2+} concentration in the solution until the 100 nM Pb^{2+} concentration was reached, from which the peak current did not increase further (Fig. 2**b**).

According to these results, the working mechanism of the 40:40 PbIP/NaTFPB membrane is hypothesized as follows. With only Pb^{2+} and/or Na^+ as the cations present in the membrane and the solution, the voltammetric peaks are ascribed to either of these two cations, knowing that the ion transfer is interconnected to the electron transfer in the POT lattice (oxidizing POT to POT^+). The total amount of Na^+ initially present in the membrane (i.e., cationic positions or the exchange capacity of the membrane) is partially or totally replaced by the Pb^{2+} from the solution during the accumulation step. As the Pb^{2+} is increased in the

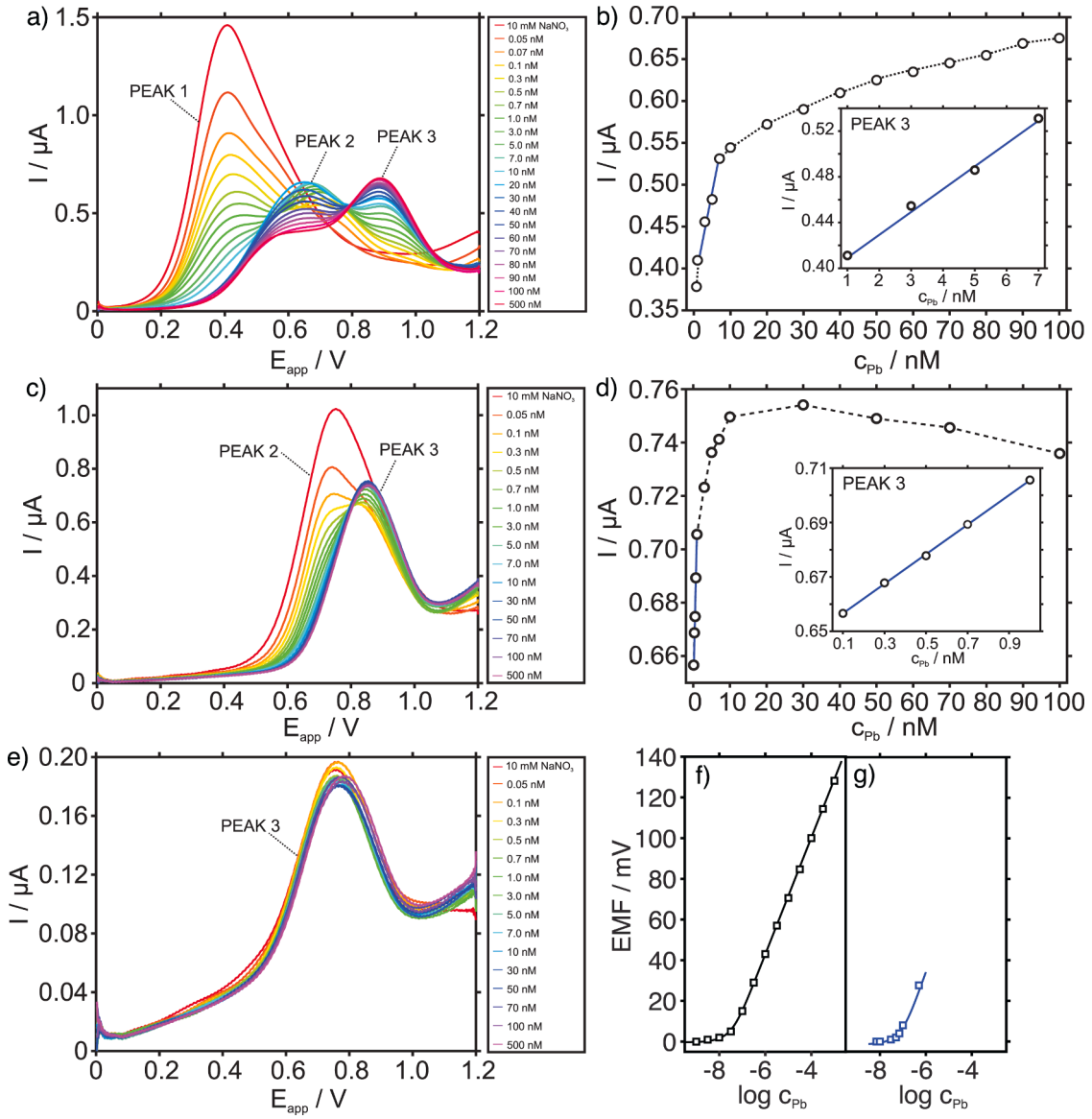

Fig. 2. Results for the lead-selective electrode. **(a)** Voltammograms with the membrane MI (40:40 PbIP:NaTFPB molar ratio) at increasing Pb^{2+} concentration in the sample solution. **(b)** Change in the current of *Peak 3* versus the Pb^{2+} concentration. Inset: linear response region. **(c)** Voltammograms with the membrane MII (80:20 PbIP:NaTFPB molar ratio) at increasing Pb^{2+} concentration in the sample solution. **(d)** Change in the current of *Peak 3* with the Pb^{2+} concentration. Inset: linear response region. **(e)** Voltammograms with the membrane MIII (80:10 PbIP:NaTFPB molar ratio) at increasing Pb^{2+} concentration in the sample solution. **(f)** Calibration graph for a potentiometrtic all-solid-state lead-selective electrode. **(g)** Calibration graph for the voltammetric lead-selective electrode prepared with membrane MIII, corresponding to the peak potentials in **Fig. 2e**.

solution, the replacement degree increases, and this is manifested in the Na^+ peak decreasing while the Pb^{2+} peak(s) increase(s) [21]. Starting from the 100 nM Pb^{2+} concentration, the maximum exchange capacity of the membrane is reached via the total replacement of Na^+, and hence, it is expected that the stripping voltametric peak related to the Pb^{2+} transfer at the membrane–sample interface will not increase anymore but shifts to a more positive peak position. This occurs as a consequence of the behavior regime in the system changing from diffusion control to a pure thin-layer process. In addition, the Pb^{2+} transfer at the membrane–sample interface seems to occur through two different paths, as observed with the appearance of *Peak 2* and *Peak 3*.

The fact that *Peak 2* appears at a lower potential than *Peak 3* and from lower Pb^{2+} concentrations indicates that *Peak 2* relates to a more favorable release of Pb^{2+} from the membrane to the solution compared to *Peak 3*. The two peaks most likely correspond to two different Pb-ionophore stoichiometries. In principle, the preferred stoichiometry is 1:1, but others are known to be possible, such as 1:3 [26,27]. In addition, *Peak 3* was found to gradually increase with the Pb^{2+} concentration in the solution, until the membrane was totally filled (i.e., from 0.3 to 90 nM). Furthermore, it seems that a rather good linearity is present from 1 to 7 nM, which could be further used for analytical purposes (inset in Fig. 2**b**): $I_{Pb} = 1.921 \times 10^7 c_{Pb} + 0.3935$, $R^2 = 0.9852$, with I_{Pb} in µA and in c_{Pb} in molar.

Fig. 2**c** displays the stripping voltammograms for the 80:20 PbIP/NaTFPB membrane (MII). Instead of the peak related to the Na^+ transfer (*Peak 1*, ca. 400 mV), the voltammogram corresponding to the background solution showed a peak at 752 mV, fairly coinciding with the position of *Peak 2* (751 mV) in the 40:40 PbIP/NaTFPB membrane (MI, Fig. 2**a**). Accordingly, the peak observed for the background solution is likely to be attributable to traces of Pb^{2+} remaining in the electrochemical cell (mainly the beaker), even though an exhaustive cleaning process was carried out before the experiment (see the Experimental section). The peak corresponding to the background (also labeled as *Peak 2* because of its correspondence with the previous membrane) was

found to gradually decrease with the Pb^{2+} concentration in the sample solution, until it disappeared at a Pb^{2+} concentration equal to 1 nM. In addition, from the very first addition of Pb^{2+} to the solution, a peak at 840 mV was shown, which was close to the potential window for *Peak 3* in membrane MI, and thus, the same label was assigned. The current of *Peak 3* was found to gradually increase with the Pb^{2+} concentration in the sample until a 10 nM concentration is reached, beyond which point the current remains almost constant (Fig. 2**d**). Overall, the total replacement of Na^+ by Pb^{2+} manifests from the initial Pb^{2+} concentration (0.05 nM), and it is distributed between two different transfers across the membrane *(Peak 2* and *Peak 3)*. An increase in the Pb^{2+} concentration is materialized as a relocation of the charge destined for each peak, favoring the event related to *Peak 3*, whose current was found to exhibit excellent linearity from 0.1 to 1 nM Pb^{2+} concentration (inset in Fig. 2**d**): $I_{Pb} = 5.393 \times 10^7 c_{Pb} + 0.6516$, $R^2 = 0.9989$, with I_{Pb} in μA and c_{Pb} in molar.

Fig. 2**e** depicts the stripping voltammograms for the 80:10 PbIP/NaTFPB membrane (MIII). As with the membrane MII, the voltammogram corresponding to the background solution displayed a peak at 761 mV, a value somewhere between *Peak 2* and *Peak 3*. However, the peak current remained almost invariable with increasing Pb^{2+} concentration in the sample solution, and hence, this was assigned as *Peak 3*. On the other hand, the peak shifted toward more positive potentials in the concentration range from 50 to 500 nM. Interestingly, the difference in the peak potential of these two concentrations was approximately 28 mV (from 762.8 to 791.3 mV), which follows the Nernstian behavior expected for a double-charged cation, i.e., 28.5 mV (very close to the ideal value of 29.6 mV) per activity decade. Overall, the system behaves under a thin-layer regime, i.e., no mass transport limitation in the membrane nor solution within the entire tested Pb^{2+} concentration range and displayed a Nernstian behavior from a 50 nM Pb^{2+} concentration. From the very first experiment, the Na^+ initially presents in the membrane is entirely replaced by Pb^{2+} (contamination traces in the background solution), and thus, only the Pb^{2+} transfer peak *(Peak 3)* is displayed in the stripping voltammograms.

Regarding the shift found for the peak position, similar behavior was observed for other electrodes in the thin-layer regime [25]: The potential associated with the ion transfer remains constant until a certain ion concentration is reached in the sample solution. This behavior is indeed in total analogy with potentiometric ISEs. In this regards, Fig. 2**f** presents the potentiometric response of a traditional all-solid-state lead-selective electrode (black line), together with that obtained with the voltammetric electrode consisting of membrane MIII (blue line). In both cases, there is a non-responsive zone after which the electrode starts exhibiting Nernstian behavior (slope of 28.2 mV dec^{-1} for potentiometry and 28.5 mV dec^{-1} for voltammetry). Evidently, the two electrodes behave very similarly, and therefore, the use of the voltammetry lead-selective electrode does not seem to provide any performance advantage *a priori*.

A global comparison of the results observed with the three membranes for lead detection revealed that as the NaTFPB concentration in the membrane is reduced, entire replacement of Na^+ (i.e., exchange capacity) is achieved at a lower Pb^{2+} concentration in the solution. Moreover, the process associated with the *Peak 3* is promoted over that manifested in *Peak 2*, and therefore, we can conclude that the Pb^{2+} binding in the membrane that is associated with *Peak 3* is more energetically favorable than that in *Peak 2:* i.e., preferred versus non-preferred lead-ionophore stoichiometry. In essence, as demonstrated in previous studies, at a reduced NaTFPB amount, only the most favorable ion transfers occur at the sample-membrane interface, and hence, this should be the case for *Peak 3* [18]. For example, in a membrane containing three ionophores for Li^+, Na^+ and K^+ (with the corresponding cation-ionophore binding constants being $Li^+ < Na^+ < K^+$), the Li^+ peak is only observed from a certain $TFPB^-$ amount in the membrane, whereas the K^+ peak is always present, regardless of the $TFPB^-$ amount. While it is evident that some hints about the overall response of the system are revealed at different PbIP/NaTFPB molar ratios, the fact that there are two peaks associated with the Pb^{2+} transfer complicates the interpretation of the results. In addition, it is difficult to calculate the charge under the peaks correctly because of the high level of overlap between *Peak 2* and *Peak 3*, which could provide more evidence about the response principle. On the other hand, from an analytical point of view, it is important to recall the excellent linear range of response achieved with membrane MII (80:20 ratio) for concentrations from 0.1 nM to 1 nM Pb^{2+}.

3.2. Response of the copper-selective electrode prepared with membranes containing different ionophore/exchanger ratios

Fig. 3 presents the stripping voltammograms for membranes containing CuIP/NaTFPB in molar ratios of 40:40 (MIV) and 80:20 (MV) at increasing Cu^{2+} concentrations (from 0.05 nM to 5 μM) in a 10 mM $NaNO_3$ background solution. Inspecting first the MIV membrane (Fig. 3**a**), there is only one peak at 261 mV *(Peak 1)* in the voltammogram corresponding to the background solution, which is attributable to the Na^+ transfer. Note that the peak potential is lower and the peak width is narrower than that displayed by the lead-selective electrode with the same membrane composition (261 mV versus 407 mV for the peak height and 144 mV versus 302 mV for the half peak width for the copper- and lead-selective electrodes, respectively). This indicates that the Na^+ transport from the membrane to the solution is more energetically favorable in the copper-selective electrode than in the lead one. The lead ionophore probably binds the Na^+ to some extent, in contrast to the copper ionophore, and this explains Na^+ expulsion occurring at a higher potential.

At increasing Cu^{2+} concentrations in the sample solution, the peak current for *Peak 1* was found to gradually decrease, whereas a new peak appeared at 842 mV *(Peak 2)* and increased until the Cu^{2+} concentration in the sample was 1 μM, beyond which point the peak kept constant (Fig. 3**b**). Although the position of the Na^+ peak *(Peak 1)* is rather well-maintained (261–268 mV) with increasing Cu^{2+} concentration, the Cu^{2+} peak *(Peak 2)* slightly shifted to less positive potentials, ranging from 842 to 884 mV and then, at a 30 nM Cu^{2+} concentration, it returned to the original peak position (from 884 to 850 mV). Furthermore, the increase in the current of *Peak 2* exhibits excellent linearity from 1 to 50 nM Cu^{2+} concentration (inset in Fig. 3**b**): $I_{Cu} = 4.589 \times 10^6 c_{Cu} + 0.1829$; $R^2 = 0.9992$, with I_{Cu} expressed in μA and c_{Cu} in molar. From the 1 μM Cu^{2+} concentration, the cationic positions in the membrane are totally filled by Cu^{2+} and hence, it is expected that the Cu^{2+} peak does not increase anymore but rather shifts to more positive potentials according to a Nernst behavior, because of the thin-layer regime of the system. Nevertheless, such a shift was not observed in the tested Cu^{2+} concentration range, but is expected to appear at higher Cu^{2+} concentrations in the solution.

Fig. 3**c** depicts the stripping voltammograms for the 80:20 CuIP/NaTFPB membrane (MV), which indeed qualitatively behaves very similarly to the previous membrane. *Peak 1,* assigned to Na^+ transfer, appears at 325 mV in the voltammogram in the background solution and decreases at increasing Cu^{2+} concentrations (Fig. 3**d**), with the peak potential remaining almost invariable (317–325 mV). *Peak 2*, assigned to Cu^{2+} transfer, appears at 890 mV for the 0.05 nM Cu^{2+} concentration, and the current gradually increases over the entire concentration range tested in the experiment (Fig. 3**d**). Then, for the Na^+ peak (*Peak 1*), the peak potential is well-maintained (890–905 mV). The increase in the current of *Peak 2* displays good linearity from 0.1 to 1 nM Cu^{2+} concentration (inset in Fig. 3 d): $I_{Cu} = 4.575 \times 10^7 c_{Cu} + 0.1919$; $R^2 = 0.9972$, with I_{Cu} expressed in μA and c_{Cu} in molar. As with the lead-selective electrode, a decrease in the NaTFPB content, together with an increase in the IP/NaTFPB molar ratio in the membrane, translates into a considerable decrease in the linear range of response for Cu^{2+}. Indeed, the linear range is the same for copper- and lead-selective electrodes, based on membranes with equivalent composition, i.e.,

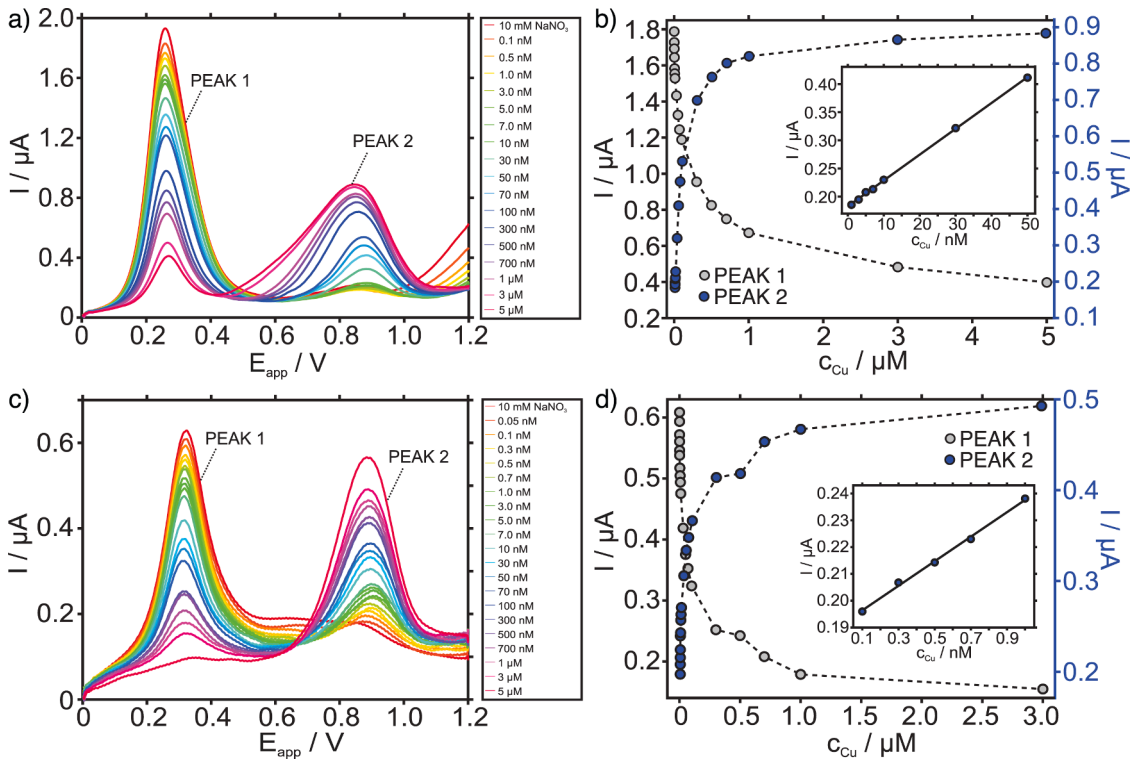

Fig. 3. Results for the copper-selective electrode. **(a)** Voltammograms with the membrane MIV (40:40 CuIP:NaTFPB molar ratio) at increasing Cu^{2+} concentration in the sample solution. **(b)** Change in the current of *Peak 2* with Cu^{2+} concentration. Inset: linear response region. **(c)** Voltammograms with the membrane MV (80:20 Cu-IP:NaTFPB molar ratio) at increasing Cu^{2+} concentration in the sample solution. **(d)** Change in the current of *Peak 2* with Cu^{2+} concentration. Inset: linear response region.

80:20 IP:NaTFPB.

However, in the case of the copper-selective electrode, the sensitivity is almost ten times lower than that for the lead-selective electrode. This may indicate that, at the same experimental conditions, Pb^{2+} expelled from the membrane to the solution somehow becomes more favorable at increasing concentrations in the solution than Cu^{2+}. The lower ionic radius of Cu^{2+} probably facilitates its retention in the membrane with respect to Pb^{2+}. Some other explanation related to the diffusional nature of the ion transfer process at the membrane–sample interface may be also acceptable. Overall, the results for the copper-selective electrode confirm that an increase in the IP/NaTFPB molar ratio in membranes with low exchange capacity favors the detection of trace concentrations of heavy metals, even at the subnanomolar level and in such a concentrated background as 10 mM $NaNO_3$.

Inspecting the charge under the Na^+ and Cu^{2+} peaks in the two investigated membranes (MIV and MV with 40:40 and 80:20 CuIP: NaTFPB), it was found that the Na^+/Cu^{2+} peak charge ratio (Q_{Na}/Q_{Cu}) varied depending on both the NaTFPB concentration in the membrane and the Cu^{2+} concentration in the sample solution, as shown in Fig. 4**a**. At low Cu^{2+} concentrations, a lower NaTFPB content manifests as a smaller Na^+ peak (smaller Q_{Na}) while this less affected the Cu^{2+} peak (similar Q_{Cu}), which generates a lower Q_{Na}/Q_{Cu}. This means that the Cu^{2+} transferred is favored over Na^+ transfer at a lower exchange capacity in the membrane, which is a direct consequence of the enhanced Cu^{2+} accumulation over Na^+ during the accumulation step. The behavior of the charge is exemplified in Fig. 4**b** by overlapping of the voltammograms obtained with membranes MIV and MV at a 30 nM Cu^{2+} concentration: The charge under *Peak 1* is ca. 6 times lower for MV than

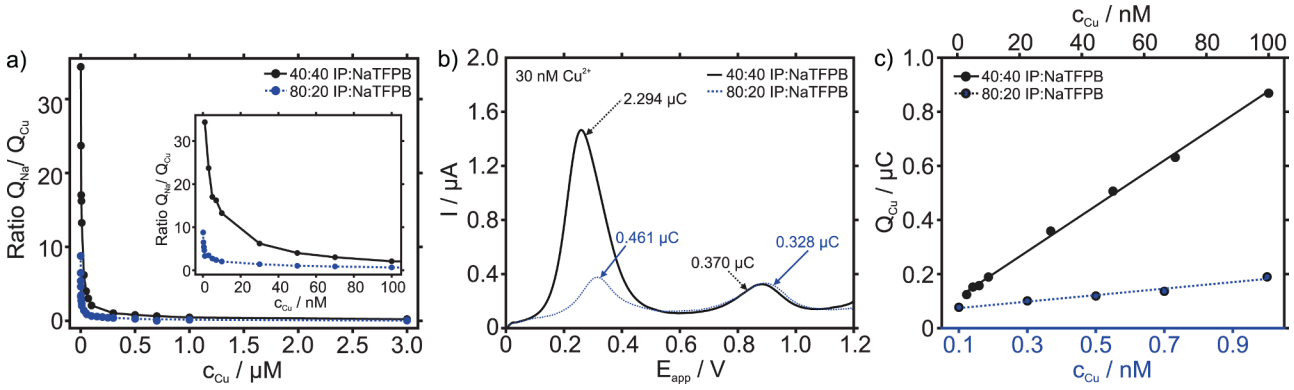

Fig. 4. **(a)** Ratio of Q_{Na}/Q_{Cu} versus Cu^{2+} concentration observed with membranes MIV and MV, 40:40 and 80:20 CuIP/NaTFPB molar ratio, respectively. Inset: magnification at lower concentrations. **(b)** Voltammograms for membranes MIV and MV at 30 nM Cu^{2+} concentration. **(c)** Linear range of response for Q_{Cu}. Calculations were performed from data in Fig. 3**a** and **c**.

MIV, whereas the charge is approximately the same for *Peak 2* for either membrane.

The Cu^{2+} concentration at which the Q_{Na}/Q_{Cu} is less than or equal to 1 (i.e., at which Q_{Cu} becomes greater than or equal to Q_{Na}) was 500 nM for membrane MIV and 100 nM for membrane MV. Furthermore, Q_{Cu} was found to presemt acceptable linearity within the ranges of 3–100 nM and 0.1–0.7 nM for MIV and mV, respectively (Fig. 4**c**): $Q_{Cu} = 7.6 \times 10^{-3} c_{Cu} + 0.112$; $R^2 = 0.9959$ for MIV and $Q_{Cu} = 9.8 \times 10^{-2} c_{Cu} + 0.071$; $R^2 = 0.9939$ for MV with Q_{Cu} expressed in μC and c_{Cu} in nM. Importantly, these relationships for the peak charge could be exploited for analytical purposes. In contrast to the lead membranes, the investigation of a further decrease of the NaTFPB amount to confirm the mentioned effect was not plausible, as the voltammetric response became very small and too noisy to be properly followed and interpreted.

3.3. Response of the silver-selective electrode prepared with membranes containing different ionophore/exchanger ratios

Fig. 5 presents the stripping voltammograms for membranes containing AgIP/NaTFPB at molar ratios of 80:40 (MVI) and 80:20 (MVII) with increasing Ag^+ concentration (from 0.05 to 300 or 70 nM, respectively) in a 10 mM $NaNO_3$ background solution. The 80:40 ratio was selected for the first experiments because this is the composition traditionally used in the corresponding potentiometric ISE (i.e., 2:1 ionophore:NaTFPB molar ratio) [28]. As observed in Fig. 5**a**, the silver-selective electrode prepared with such a membrane composition (MVI) displayed one peak at 298 mV (*Peak 1*) in the background solution, which is attributable to Na^+ transfer. The peak position is rather similar as that observed for the Na^+ peak displayed in the copper-selective electrode. The peak starts to decrease with increasing Ag^+ concentration in the sample solution, coinciding with the appearance and growth of a peak at 634 mV *(Peak 2)*, which was assigned to the Ag^+ transfer at the membrane–sample interface (Fig. 5**b**). The Ag^+ peak current reaches a constant value at a 150 nM Ag^+ concentration, indicating that the membrane is entirely filled by Ag^+. The current for *Peak 2* shows a linear relationship for Ag^+ concentrations in the sample solution from 10 to 60 nM (inset in Fig. 5**b**): $I_{Ag} = 3.8 \times 10^6 c_{Ag} + 0.3982$; $R^2 = 0.9824$ with I_{Ag} expressed in μA and c_{Ag} in molar.

With respect to the peak positions, *Peak 1* remains at a rather constant potential (297–315 mV), while *Peak 2* exhibits a slight shift from 634 mV to 664 mV with increasing Ag^+ concentration in the solution. As the Ag^+ is increased in the solution, the replacement degree of the cationic positions in the membrane increases, and thus, the peak associated with the stripping of Ag^+ increases [21]. From a 150 nM Ag^+ concentration, the membrane is fully filled by Ag^+, and hence, it is expected that the corresponding stripping voltametric peak will not increase any more but rather shifts to more positive potentials, because of the thin-layer regime of the system. Such a shift was not observed in the tested Ag^+ concentration range but may appear at higher concentrations.

This mechanism also applies to the membrane MVII with 80:20 AgIP/NaTFPB but differs in the Ag^+ concentration at which saturation is reached (30 nM). *Peak 1,* assigned to Na^+ transfer, appears at 307 mV in the voltammogram in the background solution and decreases at increasing Ag^+ concentrations (Fig. 5**c**), with the peak potential remaining rather invariable (307–342 mV). *Peak 2*, assigned to Ag^+ transfer, appears at 637 mV, and the current gradually increases until a 30 nM Ag^+ concentration is reached in the solution (Fig. 5**d**). The peak potential was well-maintained (635 – 634 mV) for this peak. The increase in the current of *Peak 2* presents rather good linearity from 0.5 to 25 nM Ag^+ concentration (inset in Fig. 5**d**): $I_{Ag} = 3.65 \times 10^6 c_{Ag} +$

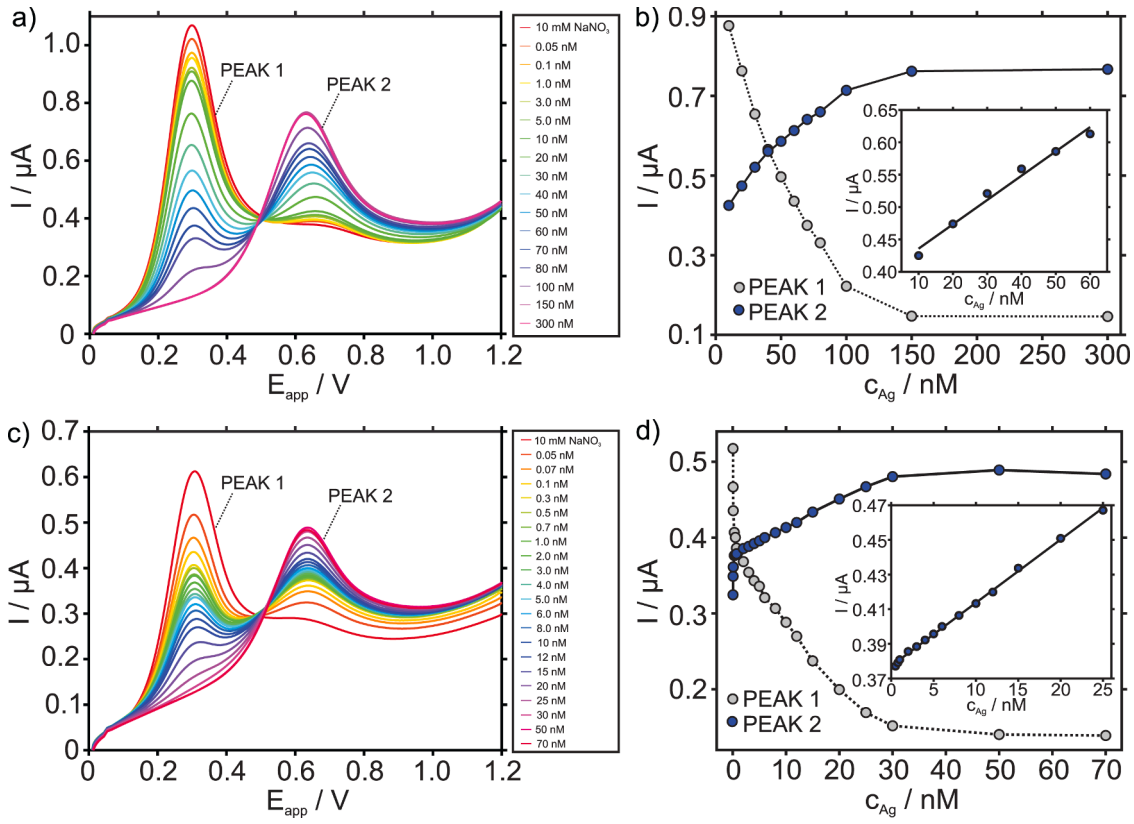

Fig. 5. Results for the silver-selective electrode. **(a)** Voltammograms for the membrane MVI (80:40 AgIP:NaTFPB molar ratio) with increasing Ag^+ concentration in the sample solution. **(b)** Change in the current of *Peak 2* with Ag^+ concentration. Inset: linear response region. **(c)** Voltammograms for the membrane MVII (80:20 AgIP:NaTFPB molar ratio) with increasing Ag^+ concentration in the sample solution. **(d)** Change in the current of *Peak 2* with Ag^+ concentration. Inset: linear response region.

0.3772; $R^2 = 0.9986$ with I_{Ag} expressed in μA and c_{Ag} in molar.

As with the lead- and copper-selective electrodes based on an 80:20 AgIP/NaTFPB membrane composition, the increase in the IP/exchanger molar ratio in the membrane translates into a linear range of response at lower Ag^+ concentrations and indeed within the nanomolar levels. Nevertheless, for the same ionophore:NaTFPB ratio (80:20), the lead and copper membranes demonstrated a sensitivity (slope) almost ten times higher than silver and a slightly lower concentration at the initiation of the linear range of response. On the other hand, the silver membrane yielded a much wider linear range of response than the other two membranes. The differences described can be related to the fact that we are comparing monovalent and divalent cations, and thus, the same charge capacity of the membrane (i.e., the same $TFPB^-$ amount) is used for the exchange of either one (Pb^{2+} and Cu^{2+}) or two (Ag^+) molecules. Thus, the change in the peak current for the same concentration change is expected to be lower for Ag^+ than for Pb^{2+} and Cu^{2+}. In other words, the change in the peak current per concentration unit will be lower for monovalent than for divalent cations, which is an advantage over potentiometric measurements, for which the opposite is true.

With respect to the charge of the two silver membranes, the Na^+/Ag^+ peak charge ratio (Q_{Na}/Q_{Ag}) is plotted in Fig. 6**a** against Ag^+ concentration in the solution. A trend similar to that for the copper membranes can be observed, where a lower NaTFPB content corresponds to a lower Q_{Na}/Q_{Ag} ratio at low Ag^+ concentrations. This behavior confirms that the accumulation of the target ions is promoted at a lower exchange capacity in the membrane. As the Ag^+ concentration gradually increases, the Q_{Na}/Q_{Ag} ratios for the two membranes were found to decrease and finally reach the same value after 70 nM Ag^+ concentration. Fig. 6**b** displays the linear responses of Q_{Ag} in the ranges of 10–100 nM and 0.5–30 nM for MVI and MVII, respectively, with the linear fittings being $Q_{Ag} = 9.6 \times 10^{-3} c_{Ag} + 0.0143$; $R^2 = 0.9967$ for MVI and $Q_{Ag} = 1.413 \times 10^{-2} c_{Ag} + 0.1812$; $R^2 = 0.9977$ for MVII, with Q_{Ag} expressed in μC and c_{Ag} in nM. Comparing the slopes observed for the 80:20 silver membrane with those calculated for the copper membrane containing the same IP/exchanger ratio, similar values are identified. Advantageously, these relationships with the peak charge could be exploited for analytical purposes. Investigation of a further decrease in the NaTFPB amount in the silver-selective membranes to confirm the favorable effect in the linear range of response was not plausible, as the voltammetric response became very small and too noisy to be properly followed and interpreted.

3.4. Exploring the possibility of analyzing multiple heavy metal ions with the developed electrodes

Having investigated the behavior of each individual electrode at different IP/exchanger molar ratios, the feasibility of a multi-analyte approach was then investigated. Considering first a membrane that could be based on more than one ionophore, and assuming that, ideally, this membrane will present an individual peak for each cation in the solution (i.e., Na^+, Pb^{2+}, Cu^{2+} and Ag^+), we overlapped the individual voltammograms displayed by the corresponding 80:20 IP/NaTFPB membranes at the same concentration for each cation (5 nM, a concentration within the linear range of response of all three) in Fig. 7**a,** in order to understand whether the simultaneous detection of all three was possible. In principle, it seems feasible to introduce either Ag^+/Pb^{2+} ionophores or Ag^+/Cu^{2+} ionophores simultaneously into the membrane, since it is evident that the peaks for Pb^{2+} and Cu^{2+} will overlap in a membrane containing Pb^{2+} and Cu^{2+} ionophores. Effectively, while the peaks for Pb^{2+} and Cu^{2+} transfer appear at a very similar potential, that for Ag^+ is expected to be rather well separated from these two peaks and also from that obtained for the Na^+ present in the background.

Fig. 7**b** shows the semi-empirical simulation of the voltammograms that will be ideally obtained with a membrane based on the three ionophores in a Na^+ background. Briefly, Eq. (1) is used to calculate the ratio of oxidized POT (with respect to the total amount that could be oxidized) $c_{POT^+}/c^{Total}_{TFPB^-}$ upon application of a linear sweep potential (E_{app}):

$$Y = A_5 + \frac{A_1 - A_2}{1 + e^{\left(x - x_{0,1}/k_1\right)}} + \frac{A_2 - A_3}{1 + e^{\left(x - x_{0,2}/k_2\right)}} + \frac{A_3 - A_4}{1 + e^{\left(x - x_{0,3}/k_3\right)}} + \frac{A_4 - A_5}{1 + e^{\left(x - x_{0,4}/k_4\right)}} \quad (1)$$

where $Y = c_{POT^+}/c^{Total}_{TFPB^-}$; $x = E_{app}$; A_1, A_2, A_3, A_4 *and* A_5 are distribution parameters that weight each mathematical term; $x_{0,1}$, $x_{0,2}$, $x_{0,3}$ *and* $x_{0,4}$ are the standard ion-transfer potentials for the ions; and k_1, k_2, k_3 *and* k_4 are related to the charge transfer process in the POT lattice involved in each of the ion transfer with $1/k = n_{POT}F/RT$ (where F is the Faraday constant, R is the gas constant, T is the absolute temperature and n_{POT} is the average number of electrons transferred at the electrode surface in going from POT^0 to POT^+) [19,29].

As we have demonstrated previously [19,29], the mathematical Sigmoidal–Boltzmann model serves to calculate how the POT^+ is gradually generated upon the applied potential, which displays a sigmoid-shaped behavior. Moreover, a sigmoid part applies to every different ion transfer and can be combined together in a mathematical equation in the form of Eq. (2), with the latter being transformed into Eq. (1) for $z = 4$ (i.e., the number of ion transfers) and n *and* $n+1$ being two consecutive peaks.

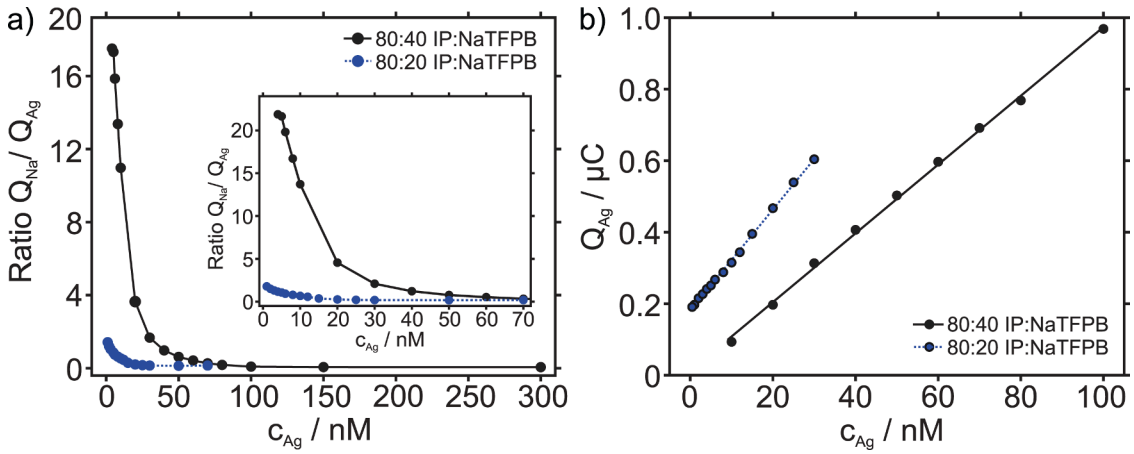

Fig. 6. (a) Ratio of Q_{Na}/Q_{Ag} observed at increasing Ag^+ concentrations for membranes MVI and MVII, 80:40 and 80:20 AgIP/NaTFPB molar ratios, respectively. Inset: magnification at lower concentrations. **(b)** Linear range of response for Q_{Ag}. Data from Fig. 5**a** and **c**.

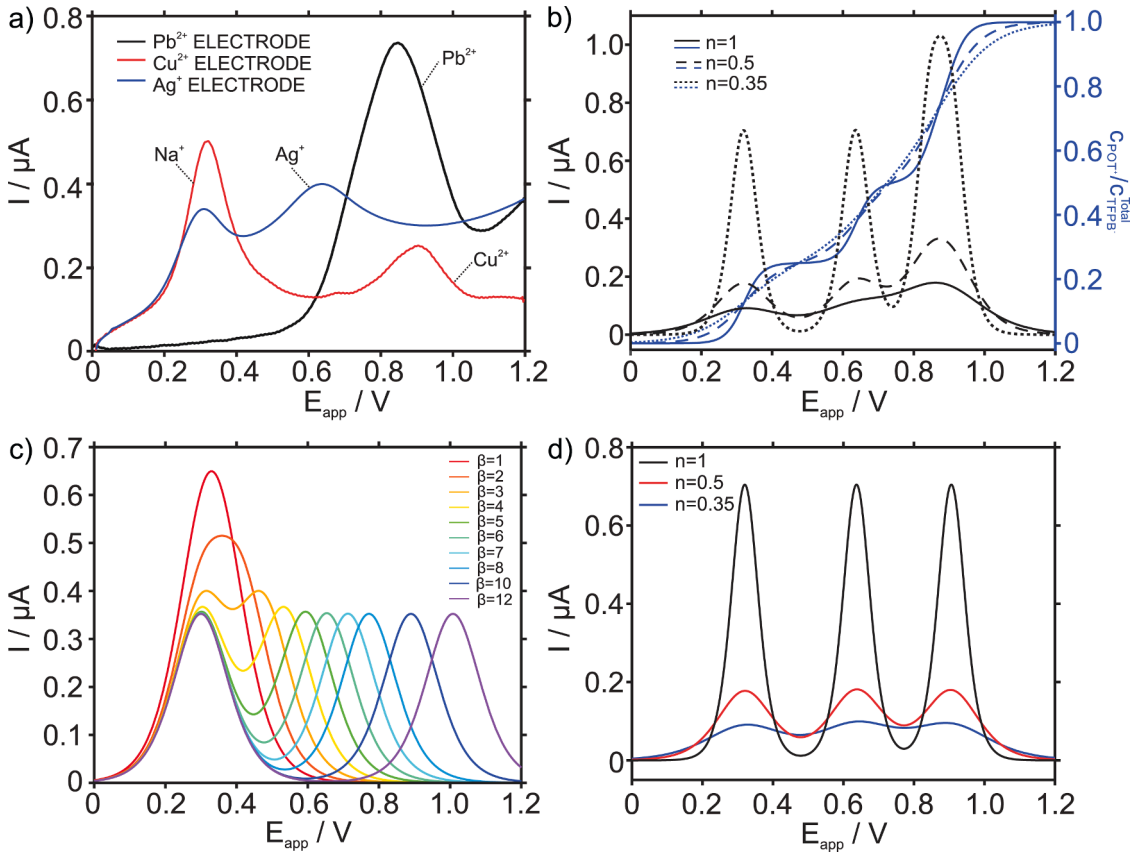

Fig. 7. **(a)** Stripping voltammograms for 5 mM concentrations of Ag^+, Cu^{2+} and Pb^{2+} in 10 mM $NaNO_3$ background solutions with electrodes based on membranes containing an 80:20 IP/exchanger molar ratio of the corresponding ionophore. **(b)** Calculated $c_{POT^+}/c^{Total}_{TFPB^-}$ and corresponding voltammograms for a membrane based on silver, copper and lead ionophores and considering n_{POT} = *0.35, 0.5* and *1*. **(c)** Calculated voltammograms for a membrane based on ionophores presenting increasing binding constant with the ion analyte (assuming n_{POT} = 0.5). **(d)** Calculated voltammograms for a membrane containing silver and copper ionophores based on n_{POT} = *0.35, 0.5* and *1*.

$$Y = A_{z+1} + \sum_{n=1}^{z} \frac{A_n - A_{n+1}}{1 + e^{\left(x - x_{0,n}/k_n\right)}} \tag{2}$$

Based on the results shown in Fig. 7**a**, the peak potential for each ion transfer was set to 320 mV for Na^+ *(z=1)*, 637 mV for Ag^+ *(z=2)*, 847 mV for Pb^{2+} *(z=3)* and 906 mV for Cu^{2+} *(z=4)*, these values corresponding to $x_{0,1}$, $x_{0,2}$, $x_{0,3}$ *and* $x_{0,4}$, respectively, in Eq. (1). In addition, the total available charge in the membrane is considered to be equally distributed among all the peaks, and thus $A_1 = 0$, $A_2 = 0.25$, $A_3 = 0.50$,$A_4 = 0.75$ and $A_5 = 1$. Finally, values of n_{POT} = 0.35, 0.5 and 1 and values of $k_1 = k_2 = k_3 = k_4$ = 73.3, 51.4 and 25.7 mV were considered. $c_{POT^+}/c^{Total}_{TFPB^-}$ was converted into the corresponding voltammograms by derivation of Eq. (1) and according to Eq. (3), which defines the current generated on E_{app}, this being the same for all points in the system:

$$i = n_{POT} F A d_{POT} \frac{\delta c_{POT^+}}{\delta t} \tag{3}$$

where $\frac{\delta c_{POT^+}}{\delta t} = c_{POT^+}/c^{Total}_{TFPB^-}$ and d_{POT} is the thickness of the POT film in the electrode (approximately 60 nm) [30].

As shown in Fig. 7**b**, for all of the tested n_{POT} values, there is considerable overlap between the Pb^{2+} and Cu^{2+} peaks for the same concentrations of the two. The overlap is more prominent for lower values of n_{POT}. In addition, the degree of overlap will be higher when one of the cations is present at a higher concentration, which is indeed expected in analyzing real water samples. This suggests that it is difficult to produce a membrane that simultaneously contains Pb^{2+} and Cu^{2+} ionophores to detect these two, because of the proximity in potential between these two ion-transfer processes. Thus, it is necessary to choose one of the two to incorporate into a membrane, together with the silver ionophore.

In designing a membrane containing more than one ionophore, it has been shown that it is crucial to provide the membrane with enough cation exchanger to allow all possible assisted (by the ionophores) transfers to be observed, regardless of the preference of the membrane for each ion [18]. This is a direct consequence of every ionophore having a different binding constant (β_{I-L}, with *I=cation* and *L=ionophore*) for the complex with the corresponding cation. Considering the ideal case in which enough NaTFPB is present in the membrane, this would have to be optimized experimentally. Fig. 7**c** presents the results of a simulation of voltammograms for increasing binding constants, using as a reference a peak of a non-assisted ion transfer, i.e., a cation that is not bonded or weakly bonded by the ionophore (such as Na^+ in our experiments). Notably, the peak potential for the ion transfer is related to the binding constant with the ionophore, according to Eq. (4), as recently demonstrated [29]:

$$log\beta_{I-L} = \frac{\left(E^0_{IT}\right)_{AS} - \left(E^0_{IT}\right)_{NAS}}{s_{AS} ln 10} \tag{4}$$

where $\left(E^0_{IT}\right)_{AS} - \left(E^0_{IT}\right)_{NAS}$ is the difference between the peak potentials of the assisted (AS) and non-assisted (NAS) ion transfers and s_{AS} is equal to $RT/n_{AS}F$ (where n_{AS} is the number of molecules of of I^+ involved in the ion transfer).

The voltammogram simulation results shown in Fig. 7**c** were obtained with the following values set in Eq. (2): *z=2*, $x_{0,1}$ = 300 *mV*, n_{POT}=0.5, and $x_{0,2}$ = 359, 418, 477, 536, 595, 654, 713, 772,

890 and 1008 mV. These inputs resulted in values of $\beta_{I-L} = 1,\ 2,\ 3,\ 4,\ 5,\ 6,\ 7,\ 8,\ 10$ and 12 as well as $A_1 = 0,\ A_2 = 0.50$ and $A_3 = 1$, with the rest of the parameters the same as those employed for the simulations whose results are shown in Fig. 7**b**. A value of $x_{0,1} = 300\ mV$ was selected as the reference potential, and the different $x_{0,2}$ values were calculated to cover the entire range of the β_{I-L} values to provide a complete view of the peak overlap. A value of $n_{POT} = 0.5$ was selected as an intermediate value among those used to obtain the voltammograms in Fig. 7**b**. Evidently, a higher value for n_{POT} provides a better separation for the two peaks at a lower β_{I-L} value, which is convenient for achieving maximum peak resolution and hence optimal results from an analytical perspective. As Fig. 7**c** shows, for a logarithmic binding constant value of 4, the peaks for the unassisted and assisted ion transfers are totally separated. This situation can be extrapolated to the case of two different ions of the same charge complexed by two different ionophores in the membrane. Thus, a separation of four logarithmic units between the two binding constants will, in principle, ensure that the peaks are well separated in the voltammogram.

For the case of a membrane based on Ag^+ and Cu^{2+} ionophores, Fig. 7**d** shows the simulation results for a voltammogram obtained using Eq. (2) with $z = 3$; $n_{POT} = 0.35,\ 0.5$ and 1; $x_{0,1} = 0\ mV(Na^+)$; $x_{0,2} = 637\ mV\ (Ag^+)$; $x_{0,3} = 906\ mV\ (Cu^{2+})$; $A_1 = 1$; $A_2 = 0.75$; $A_3 = 0.25$; $A_4 = 0$, and the rest of the parameters having the same values as those employed for the simulations whose results are shown in Fig. 7**b**. The separation calculated for the Ag^+ and Cu^{2+} peaks is predicted to be sufficient to provide well-defined peaks for all of the evaluated n_{POT} values. In addition, the Na^+ and Ag^+ peaks are separated sufficiently to avoid significant overlay. However, we know from previous measurements with real samples that the peak associated with the sample background may appear in the form of a broad band because of overlapping of many peaks for complex matrix samples (i.e., many different ions in the matrix apart from the analyte one) [21]. Accordingly, the simulations should be considered as approximations of real cases that may facilitate experimental planning and related investigations. In future experimental steps, it would be necessary to check the real cross selectivity (and hence overlapping possibility) of the electrode and define the concentration ranges for analytical applicability, considering that all the cations are simultaneously present in the solution.

For the case of a membrane based on Ag^+ and Pb^{2+} ionophores, it is difficult to predict the response behavior because the number of peaks will be highly dependent on the NaTFPB content of the membrane, since Pb^{2+} transfer has been shown to occur through two different paths (see above). One of the Pb^{2+} transfer paths (i.e., that at 750 mV, assigned to the non-preferred stoichiometry) lies close to the Ag^+ peak, which is not very convenient. Further experiments will be conducted in our laboratory with a focus on a single electrode based on Ag^+ and Cu^{2+} ionophores simultaneously incorporated into a membrane, in conjunction with a lead-selective electrode in a voltammetric multiple-electrode device to quantify heavy metal ions in water samples. Electrodes for other heavy metals (such as cadmium and zinc) based on other ionophores can also be considered. Ultimately, we seek to develop a voltametric device wherein the number of electrodes needed for reliable quantification is minimized and thus so too is the complexity of the signal analysis.

4. Conclusions

This work investigated the versatility of voltammetric ion-selective electrodes based on ultra-thin membranes for the detection of heavy metals ions —specifically lead, copper and silver— at nanomolar levels. Upon application of an accumulation/stripping electrochemical protocol, the exploration of the membrane composition demonstrated that formulations with a low exchange capacity and a high ionophore/exchanger ratio promote a linear range of responses for the peak current versus the ion concentration at trace levels, as low as 0.1 nM. In essence, the replacement of the cationic exchange positions in the membranes with the heavy metal ion from the solution is favored under such circumstances. On the one hand, when the initial content of the cation exchanger is lower, the total replacement is reached at a lower ion concentration. On the other hand, a greater difference between the molar content of the ionophore and the exchanger enhances the accumulation of the targeted ion in the membrane versus any other type of ion (e.g., sodium ion initially present in the membrane and in the background solution), and this in turn is manifested in a membrane response at lower concentrations. Semi-empirical simulations based on experimental peak positions observed in the stripping voltammograms, together with a recent theory developed by our group *(Electrochimica Acta 2021, 388, 138634)*, have been performed to assess the feasibility of utilization of the developed electrodes for multi-ion analytical sensing in water samples. It has been concluded that the tailoring of an electrode to measure silver and copper ions simultaneously is feasible in principle, whereas lead detection requires an extra electrode. The reason for this is that the lead ion exhibits two peaks attributable to the transfer of lead ions across the membrane that cover the vast majority of the potential window of the stripping voltammogram. These peaks overlap the transfer of any other heavy metal ion for which the electrode could be selective. Overall, this work has demonstrated considerable advances in heavy metal ion detection that may have implications in the replacement of the use of any mercury electrode.

CRediT authorship contribution statement

Kequan Xu: Methodology, Software, Validation, Formal analysis, Investigation, Data curation, Writing – original draft. **Yujie Liu:** Methodology, Software, Validation, Formal analysis, Investigation, Data curation, Writing – original draft. **Gaston A. Crespo:** Conceptualization, Methodology, Software, Resources, Writing – original draft, Writing – review & editing, Supervision. **Maria Cuartero:** Conceptualization, Methodology, Software, Validation, Formal analysis, Investigation, Resources, Data curation, Writing – original draft, Writing – review & editing, Supervision, Project administration, Funding acquisition.

Declaration of Competing Interest

The authors declare that they have no known competing financial interests or personal relationships that could have appeared to influence the work reported in this paper.

Acknowledgments

This project received funding from the European Research Council (ERC) under the European Union's Horizon 2020 Research and Innovation Programme (Grant Agreement No. 851957). K.X. and Y.L. gratefully thank the China Scholarship Council for supporting their Ph. D. studies.

References

[1] P.B. Tchounwou, C.G. Yedjou, A.K. Patlolla, D.J. Sutton, Heavy metal toxicity and the environment. molecular, clinical and environmental toxicology, Exp. Suppl. 101 (2012) 133–164.
[2] Z.L. He, X.E. Yang, P.J. Stoffella, Trace elements in agroecosystems and impacts on the environment, J. Trace Elem. Med. Biol. 19 (2005) 125–140.
[3] M. Cuartero, Electrochemical sensors for *in-situ* measurement of ions in seawater, Sens. Actuators B 334 (2021), 129635.
[4] L.A. Malik, A. Bashir, A. Qureashi, A.H. Pandith, Detection and removal of heavy metal ions: a review, Environ. Chem. Lett. 17 (2019) 1495–1521.
[5] M.L. Tercier, J. Buffle, A. Zirino, R. De Vitre, *In situ* voltammetric measurement of trace elements in lakes and oceans, Anal. Chim. Acta 237 (1990) 429–437.
[6] Idronaut, VIP system. https://www.idronaut.it/in-situ-trace-metals/vip-system/. Accessed on 5 March 2022.
[7] D.W. Arrigan, Voltammetric determination of trace metals and organics after accumulation at modified electrodes, Analyst 119 (1994) 1953–1966.

[8] K. Xu, C. Pérez-Ràfols, A. Marchoud, M. Cuartero, G.A. Crespo, Anodic stripping voltammetry with the hanging mercury crop electrode for trace metal detection in soil samples, Chemosensors 9 (2021) 107.
[9] J. Wang, Analytical Electrochemistry, John Wiley & Sons, Hoboken, NJ, USA, 2006.
[10] N. Serrano, J.M. Díaz-Cruz, C. Arino, M. Esteban, Antimony-based electrodes for analytical determinations, TrAC Trends Anal. Chem. 77 (2016) 203–213.
[11] Hub, E.S. European union reference laboratories. https://ec.europa.eu/jrc/en/eurls. Accessed on 19 February 2022).
[12] S. Sang, D. Li, H. Zhang, Y. Sun, A. Jian, Q. Zhang, W. Zhang, Facile synthesis of AgNPs on reduced graphene oxide for highly sensitive simultaneous detection of heavy metal ions, RSC Adv. 7 (2017) 21618–21624.
[13] Y. Wei, C. Gao, F.L. Meng, H.H. Li, L. Wang, J.H. Liu, X.J. Huang, SnO_2/reduced graphene oxide nanocomposite for the simultaneous electrochemical detection of cadmium (II), lead (II), copper (II), and mercury (II): An interesting favorable mutual interference, J. Phys. Chem. C 116 (2012) 1034–1041.
[14] P. Veerakumar, V. Veeramani, S.M. Chen, R. Madhu, S.B. Liu, Palladium nanoparticle incorporated porous activated carbon: electrochemical detection of toxic metal ions, ACS Appl. Mater. Interfaces 8 (2016) 1319–1326.
[15] J. Van Staden, M. Matoetoe, Simultaneous determination of copper, lead, cadmium and zinc using differential pulse anodic stripping voltammetry in a flow system, Anal. Chim. Acta 411 (2000) 201–207.
[16] A.R. Thiruppathi, B. Sidhureddy, W. Keeler, A. Chen, Facile one-pot synthesis of fluorinated graphene oxide for electrochemical sensing of heavy metal ions, Electrochem. Commun. 76 (2017) 42–46.
[17] F. Gao, N. Gao, A. Nishitani, H. Tanaka, Rod-like hydroxyapatite and Nafion nanocomposite as an electrochemical matrix for simultaneous and sensitive detection of Hg^{2+}, Cu^{2+}, Pb^{2+} and Cd^{2+}, J. Electroanal. Chem. 775 (2016) 212–218.
[18] M. Cuartero, G.A. Crespo, E. Bakker, Ionophore-based voltammetric ion activity sensing with thin layer membranes, Anal. Chem. 88 (2016) 1654–1660.
[19] Y. Liu, A. Wiorek, G.A. Crespo, M. Cuartero, Spectroelectrochemical evidence of interconnected charge and ion transfer in ultrathin membranes modulated by a redox cconducting polymer, Anal. Chem. 92 (2020) 14085–14093.
[20] K. Xu, M. Cuartero, G.A. Crespo, Lowering the limit of detection of ion-selective membranes backside contacted with a film of poly (3-octylthiophene), Sens. Actuators B 297 (2019), 126781.
[21] K. Xu, G.A. Crespo, M. Cuartero, Subnanomolar detection of ions using thin voltammetric membranes with reduced exchange capacity, Sens. Actuators B 321 (2020), 128453.
[22] D. Yuan, A.H. Anthis, M. Ghahraman Afshar, N. Pankratova, M. Cuartero, G.N. A. Crespo, E. Bakker, All-solid-state potentiometric sensors with a multiwalled carbon nanotube inner transducing layer for anion detection in environmental samples, Anal. Chem. 87 (2015) 8640–8645.
[23] S. Yu, F. Li, T. Yin, Y. Liu, D. Pan, W. Qin, A solid-contact Pb^{2+}-selective electrode using poly (2-methoxy-5-(2′-ethylhexyloxy)-p-phenylene vinylene) as ion-to-electron transducer, Anal. Chim. Acta 702 (2011) 195–198.
[24] D. Yuan, M. Cuartero, G.A. Crespo, E. Bakker, Voltammetric thin-layer ionophore-based films: part 1. Experimental evidence and numerical simulations, Anal. Chem. 89 (2017) 586–594.
[25] G.A. Crespo, M. Cuartero, E. Bakker, Thin layer ionophore-based membrane for multianalyte ion activity detection, Anal. Chem. 87 (2015) 7729–7737.
[26] M. Guziński, G. Lisak, J. Kupis, A. Jasiński, M. Bocheńska, Lead (II)-selective ionophores for ion-selective electrodes: a review, Anal. Chim. Acta 791 (2013) 1–12.
[27] A. Kamal, R. Tejpal, V. Bhalla, M. Kumar, R. Mahajan, Selective and sensitive lead (II) solid-contact potentiometric sensor based on naphthalene-sulfonamide derivative, Int. J. Environ. Sci. Technol. 12 (2015) 2567–2578.
[28] K. Xu, C. Pérez-Ràfols, M. Cuartero, G.A. Crespo, Electrochemical detection of trace silver, Electrochim. Acta 374 (2021), 137929.
[29] Y. Liu, G.A. Crespo, M. Cuartero, Semi-empirical treatment of ionophore-assisted ion-transfers in ultrathin membranes coupled to a redox conducting polymer, Electrochim. Acta 388 (2021), 138634.
[30] M. Cuartero, R.G. Acres, R. De Marco, E. Bakker, G.A. Crespo, Electrochemical ion transfer with thin films of poly (3-octylthiophene), Anal. Chem. 88 (2016) 6939–6946.